Food Hydrocolloids 145 (2023) 109080

Contents lists available at ScienceDirect

Food Hydrocolloids

journal homepage: www.elsevier.com/locate/foodhyd

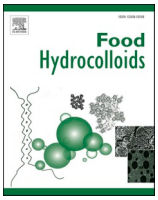

Bacterial cellulose vs. bacterial cellulose nanocrystals as stabilizer agents for O/W pickering emulsions

Agata Sommer, Hanna Staroszczyk *

Department of Chemistry, Technology and Biotechnology of Food, Faculty of Chemistry, Gdansk University of Technology, Gabriela Narutowicza 11/12, Gdańsk, Pomeranian Voivodeship, Poland

ARTICLE INFO

Keywords:
Bacterial cellulose
Pickering emulsion stabilizer
Nanocrystals
Crystal structure

ABSTRACT

The growing interest in Pickering emulsions in functional food systems resulted in the need to find suitable stabilizers for them. The work considers the use of bacterial cellulose for this purpose, and its aim was to compare the properties of disintegrated bacterial cellulose, before and after freeze-drying, and its nanocrystals obtained using H_2SO_4 under variable of time and concentration conditions. The structure of nanocrystals obtained with 30% acid was found to be still similar to that of parent cellulose, while the structure of nanocrystals obtained with 65% acid showed allomorphic transformation and the cellulose sulfates formation, regardless of the acid treatment time. Unlike nanocrystals obtained with 65% acid, those obtained with 30% acid as well as native bacterial cellulose ensured the high stability of O/W emulsion containing up to 20% olive oil. Effective stabilization of emulsions with the addition of nanocrystals obtained with the use of 30% acid was ensured by their strong surface charge density due to the presence of negatively charged sulfate groups.

1. Introduction

An emulsion is a mixture of two immiscible liquid phases, typically oil and water, one of which is dispersed uniformly in the other in the form of fine droplets. Due to various physicochemical processes, including coalescence, flocculation, Ostwald ripening, gravitational and phase separation, emulsions are thermodynamically unstable and tend to breakdown over time (Mason, Wilking, Meleson, Chang, & Graves, 2006; Ozturk & McClements, 2016). Hence, the addition of stabilizers to the emulsion is necessary. Emulsifiers (surfactants), by concentrating at the liquid-liquid phases interface, either reduce interfacial tension and lower the energy needed to form emulsions (Binks, 2007) or form a steric barrier that prevents droplet coalescence (Low, Siva, Ho, Chan, & Tey, 2020; Pang, Liu, & Zhang, 2021). In the latter case, Pickering emulsions are formed, usually stabilized with solid particles, i.e., clay, hydroxyapatite, and some organic particles (Agarwal, Phuoc, Soong, Martello, & Gupta, 2013; Capron & Cathala, 2013; Grechishcheva, Perminova, Kholodov, & Meshcheryakov, 2017). To be used as stabilizers in Pickering emulsions, the solids must be partially wettable by both the dispersed and the continuous phase of the emulsion, but not dissolved therein. Also, the surface charge of solid particles used cannot be too high and their size should be much lower than that of the emulsion droplets (Björkegren, Nordstierna, Törncrona, & Palmqvist, 2017). The commercial use of Pickering emulsions in the food industry is gaining interest due to environmental, health, and cost issues posed by surfactants used in traditional emulsions (Jia, Zheng, Xu, & Zhong, 2019). The use of non-toxic, food-grade particulates, such as polysaccharides, including cellulose, as an emulsion stabilizer, ensures not only food safety (Yan et al., 2017) but it also gives an opportunity to strategically modify the stabilizer to control its behavior in the emulsion, thus creating on-demand emulsions with specific properties (Calabrese, Courtenay, Edler, & Scott, 2018). Pickering emulsions stabilized with cellulose, which is a good source of dietary fiber, may be potential as a functional food source (Cheon, Haji, Baek, Wang, & Tam, 2023).

Cellulose is a polysaccharide derived from plants and bacteria. The molecular structure of bacterial cellulose (BC) is the same as plant cellulose, but the former is not associated with hemicellulose and lignin as is the case with the latter. This makes BC a pure form of cellulose. The polysaccharide is composed of D-glucose units linked by β-(1 → 4)-glycosidic bonds into linear chains, between of which the extensive network of intra- and inter-chains hydrogen bonds is formed. Depending on the pattern of H-bonds, four polymorphic crystalline structures are distinguished: cellulose I, II, III, and IV (Peter, 2021). Cellulose I is the crystalline cellulose with a parallel arrangement of chains in the unit

* Corresponding author.
E-mail address: hanna.staroszczyk@pg.edu.pl (H. Staroszczyk).

https://doi.org/10.1016/j.foodhyd.2023.109080
Received 28 March 2023; Received in revised form 30 June 2023; Accepted 13 July 2023
Available online 14 July 2023

Table 1
Experimental plan.

Sample no.	Levels of the variability for the input variables			Levels of the factor values			Composition of the emulsion
	x_1	x_2	x_3	Stabilizer type	Stabilizer concentration (%, w/v)	Oil concentration (%, v/v)	
1	1	0	−1	wBC	0.3	10	10% O/W0.3%wBC
2	1	1	−1	wBC	0.9	10	10% O/W0.9%wBC
3	1	0	0	wBC	0.3	20	20% O/W0.3%wBC
4	1	1	0	wBC	0.9	20	20% O/W0.9%wBC
5	1	0	1	wBC	0.3	30	30% O/W0.3%wBC
6	1	1	1	wBC	0.9	30	30% O/W0.9%wBC
7	0	0	−1	fdBC	0.3	10	10% O/W0.3%fdBC
8	0	1	−1	fdBC	0.9	10	10% O/W0.9%fdBC
9	0	0	0	fdBC	0.3	20	20% O/W0.3%fdBC
10	0	1	0	fdBC	0.9	20	20% O/W0.9%fdBC
11	0	0	1	fdBC	0.3	30	30% O/W0.3%fdBC
12	0	1	1	fdBC	0.9	30	30% O/W0.9%fdBC
13	−1	0	−1	XG	0.3	10	10% O/W0.3%fdBC
14	−1	1	−1	XG	0.9	10	10% O/W0.9%fdBC
15	−1	0	0	XG	0.3	20	20% O/W0.3%fdBC
16	−1	1	0	XG	0.9	20	20% O/W0.9%fdBC
17	−1	0	1	XG	0.3	30	30% O/W0.3%fdBC
18	−1	1	1	XG	0.9	30	30% O/W0.9%fdBC
19	–	−1	−1	–	0	10	10% O/W
20	–	−1	0	–	0	20	20% O/W
21	–	−1	1	–	0	30	30% O/W

cell. The triclinic I_α and monoclinic I_β polymorphs, with one and two chains in a unit cell structure, respectively, differ in the distribution and number of inter-chains H-bonds. Cellulose II of a monoclinic structure with two anti-parallel chains in the unit cell can be prepared in the process of regeneration (solubilization and then recrystallization) and mercerization (alkali treatment) of native cellulose (Xing, Gu, Zhang, Tu, & Hu, 2018). Cellulose III including cellulose III_I and III_{II} can be formed from cellulose I and II, respectively, by liquid ammonia treatment (Hayashi, Sufoka, Ohkita, & Watanabe, 1975). These can then be thermally treated to form cellulose IV_I and IV_{II}, respectively (Gardiner & Sarko, 1985). In regions where these H-bonds are broken, the highly ordered arrangement (crystalline structure) is lost to the disordered one (amorphous structure).

Cellulose subjected to acid (with H_2SO_4) or enzymatic (with cellulase) hydrolysis yields nanocrystals (Beltramino, Roncero, Vidal, Torres, & Valls, 2015, 2016; Gong, Li, Xu, Xiang, & Mo, 2017; Pereira & Arantes, 2020; Tang, Yang, Zhang, & Zhang, 2014; Tong, Shen, Chen, Jia, & Roux, 2020; Vasconcelos et al., 2017). During acid hydrolysis, the amorphous regions of the cellulose are attacked and hydrolyzed first, while the crystalline regions show higher resistance to this reaction. As a result, the amorphous regions of the cellulose are removed and the intact crystalline domains remain. Depending on the hydrolysis reaction conditions, i.e., the acid type and concentration, reaction time and temperature, nanostructures with different physical and mechanical properties are obtained (Vasconcelos et al., 2017). Cellulose nanocrystals have attracted a lot of interest as promising stabilizers for Pickering emulsion (Cherhal, Cousin, & Capron, 2016). Although those derived from plant cellulose have the same properties as those derived from BC, bacterial cellulose is a better source of nanocrystals than plant counterpart due to the contamination of the latter (Wang, Tavakoli, & Tang, 2019). Moreover, the high crystallinity of BC compared to plant cellulose mean that not only the nanocrystals but also native BC can be used as a Pickering emulsion stabilizer. According to Zhai, Lin, Liu, and Yang (2018), the BC used in Pickering emulsion type oil in water (O/W) has the unique ability to prevent droplet aggregation over a wide range of temperature.

The aim of the study was to compare the properties of disintegrated native BC, before and after its freeze-drying, with the properties of BC nanocrystals obtained by acid hydrolysis of the polysaccharide under variable conditions of time and concentration, used as a stabilizer of O/W Pickering emulsions. To our best knowledge, native and dried BC have not yet been compared with its nanocrystals for emulsion stabilization.

2. Experimental section

2.1. Materials

Gluconacetobacter xylinus LOCK 89 was purchased from Pure Culture Collection of the Institute of Fermentation Technology and Microbiology (Lodz University of Technology, Poland). Food grade rafined olive oil was supplied by Olio Luglio, Medsol srl (Molfett, BA, Italy) and food grade xanthan gum (XG) by Adox Group (Antoninów, Poland). All other chemicals were analytical grade, and the microbial medium ingredients – microbiology grade.

2.2. Bacterial cellulose preparation

BC membranes were synthesized by *G. xylinus* as described previously (Sommer, Staroszczyk, Sinkiewicz, & Bruździak, 2021). Briefly, bacteria were cultured for 7 days at 28 °C in a Hestrin-Schramm medium composed of 2% (w/v) glucose, 0.27% (w/v) Na_2HPO_4, 0.115% (w/v) citric acid, 0.5% (w/v) yeast extract, 0.5% (w/v) peptone K, and 1% (v/v) ethanol (Hestrin & Schramm, 1954). The obtained BC membranes were rinsed in tap water, purified in boiling 4% NaOH for 1 h, rinsed again until neutral pH was achieved, immersed in distilled water, and then sterilized at 121 °C in an autoclave (VX-75, Systec GmbH, Germany). The purified BC membranes with 99.1 ± 0.1% water content were homogenized (homogenizer MixSy, Zepter, Switzerland) until a uniform paste of wet BC (wBC) was obtained, and finally freeze-dried (freeze dryer Christ Alpha 2–4 LSC, Martin Christ Gefriertrocknungsanlagen GmbH, Germany), and ground again with a homogenizer until freeze-dried BC flakes (fdBC) were obtained.

2.3. Bacterial cellulose nanocrystals preparation

Flakes of fdBC were mixed in the ratio of 1:30 (w/v) with either 30 or 65% H_2SO_4 to give nanocrystals NBC_130 or NBC_165 and NBC_330 or NBC_365, after 1- and 3-h hydrolysis at 50 °C, respectively. After stopping the reaction with 10^{-4} M NaOH, BC nanocrystals obtained were separated from the suspension by centrifugation (9000 rpm, 25 °C, 10 min), dialyzed for 72 h, and finally freeze-dried.

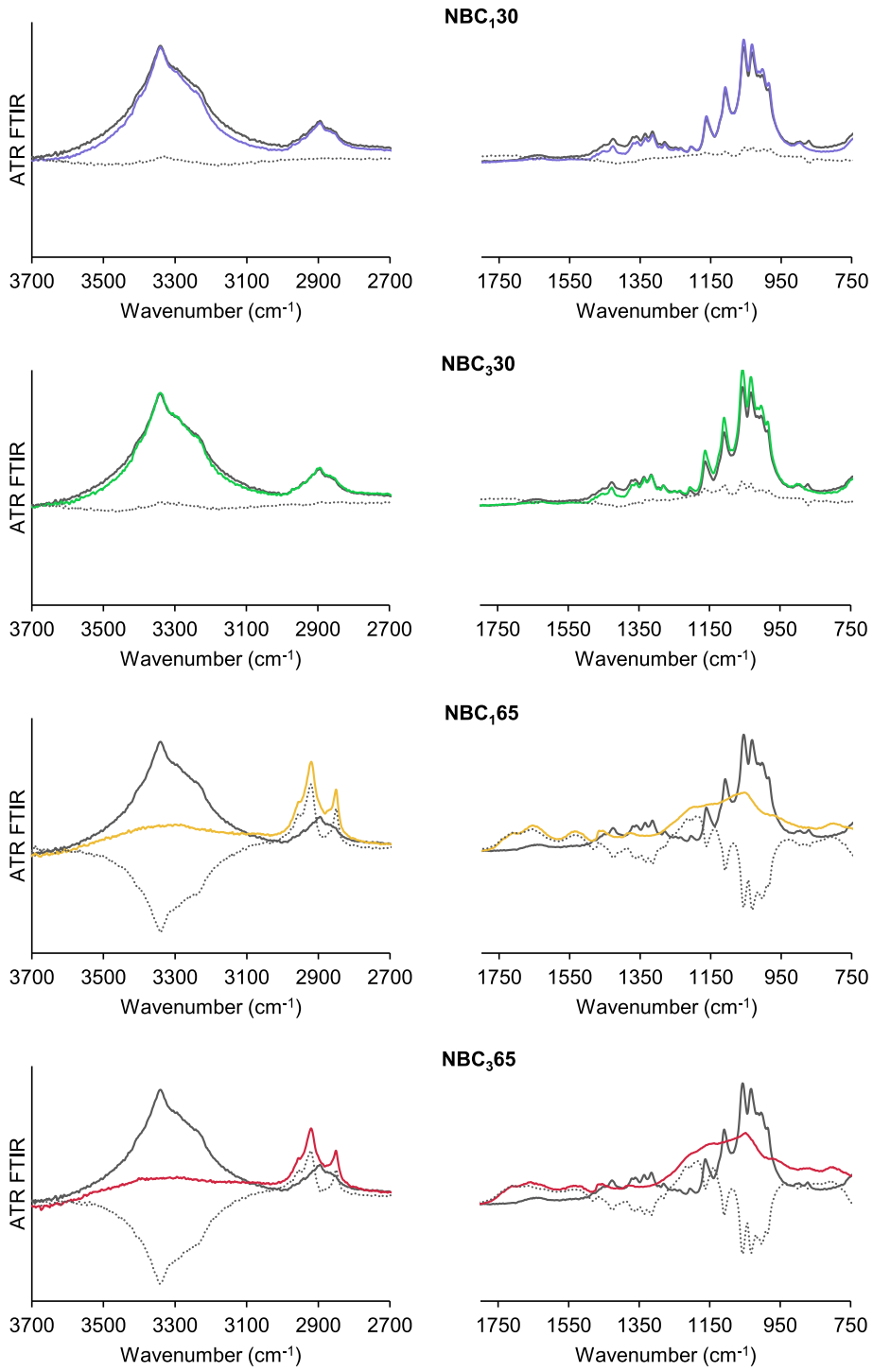

Fig. 1. ATR-FTIR spectra of BC nanocrystals: $NBC_1 30$ —, $NBC_3 30$ —, $NBC_1 65$ —, $NBC_3 65$ —, and difference spectra of the BC nanocrystal from which the spectrum of fdBC was subtracted ·····. The spectrum of fdBC — was added for comparison.

2.4. BC nanocrystal characteristics

2.4.1. Attenuated total reflectance fourier transform infrared spectroscopy (ATR FT-IR)

The ATR FT-IR spectra of $NBC_1 30$, $NBC_3 30$ and $NBC_1 65$, $NBC_3 65$ as well as fdBC were recorded on a Nicolet 8700 spectrophotometer (Thermo Electron Scientific Inc., Waltham, MA, USA), using a Golden Gate ATR accessory (Specac, Orpington, UK) equipped with a single-reflection diamond crystal. Each spectrum, recorded within 5000–500 cm^{-1} wavenumber range, was obtained by measuring and averaging 128 independent scans with 4 cm^{-1} resolution. All samples were previously homogenized in a ball mill and conditioned for 7 days in a desiccator over P_2O_5 to remove residual moisture.

Total crystallinity index (TCI) (Nelson & O'Connor, 1964a), lateral order index (LOI) (Hurtubise & Krassig, 1960), and hydrogen bond intensity index (HBI) (Kljun et al., 2011; Nada, Kamel, & El-Sakhawy, 2000) calculated from the absorbance ratios: A_{1372}/A_{2897}, A_{1430}/A_{893}, and A_{3336}/A_{1336}, respectively, were used to study the crystallinity changes caused by the hydrolysis reaction.

Table 2
Band assignment in the FT-IR spectra of fdBC and nanocrystals formed after its hydrolyzis.

Band assignment[a]	Position (cm^{-1})				
	fdBC	$NBC_1$30	$NBC_3$30	$NBC_1$65	$NBC_3$65
ν_{OH} intramolecular H-bonds for 3O···H–O5 and 2O··· H–O6	3383	3383	3383	3388	3392
ν_{OH} intramolecular H-bonds for 3O···H–O5	3340	3342	3340	3346	3332
ν_{OH} intermolecular H-bonds (corresponding to the contribution from cellulose I_β)	3317	3317	3317	3302	3315
ν_{OH} intermolecular H-bonds for 6O···H–O3' (corresponding to the contribution from cellulose I_α)	3242	3242	3242	3248	3248
ν_{CH}	2895	2897	2895	2954, 2920, 2850	2954, 2920, 2850
δ_{OH} polymer bound water	1641	1631	1631	1649	1649
δ_{OH}, δ_{CH}	1427	1427	1427	1458	1458
δ_{OH}, δ_{CH}	1361	1358	1358	1361	1361
δ_{OH}	1336	1334	1334	1342	1323
δ_{CH}	1282	1282	1282	1282	1282
$\nu_{S=O}$ of O–SO_3^-	–	–	–	1236	1236
δ_{CH}	1162	1161	1163	1163	1163
δ_{C-OH} of C2–OH	1109	1109	1109	1109	1109
δ_{C-OH} of C3–OH	1057	1057	1057	1055	1047
ν_{C-O} of C6–OH	1032	1032	1034		
ν_{C-O}	1005	1003	1005	1005	1005
ν_{C-O}	985	985	985	985	985
β-glycosidic linkage	897	–	–	–	–
ν_{C-O-S} of C–O–SO_3^-	–	–	–	800	800
I_α, δ_{OH} out-of-plane	744	742	744	758	758
I_β, δ_{OH} out-of-plane	696	696	696	700	702

[a] According to Cheng, Liu, Feng, Xie, & Zhan, 2017; de Moraes Crizel, Haas Costa, de Oliveira Rios, & Hickmann Flôres, 2016; Goh et al., 2012; Kruer-Zerhusen et al., 2018; Liang et al., 2018; Oh, Yoo, Shin, Kim, et al., 2005; Oh, Yoo, Shin, & Seo, 2005; Shah, Ul-Islam, Khattak, & Park, 2013; Shahabi-Ghahafarrokhi, Khodaiyan, Mousavi, & Yousefi, 2015; Sommer, Dederko-Kantowicz et al., 2021; Sommer, Staroszczyk, et al., 2021; Surma-Ślusarska, Presler, & Danielewicz, 2008; Ul-Islam, Khan, & Park, 2012; Vasconcelos et al., 2017; Yang, Du, Wen, Li, & Hu, 2003.

Table 3
The crystallinity changes caused by the hydrolysis of fdBC after 1 and 3 h with 30% ($NBC_1$30 and $NBC_3$30) and 65% ($NBC_1$65 and $NBC_3$65) H_2SO_4.

Index	fdBC	$NBC_1$30	$NBC_3$30	$NBC_1$65	$NBC_3$65
TCI	1.69 ± 0.01	1.25 ± 0.04	1.23 ± 0.03	0.93 ± 0.00	1.14 ± 0.00
LOI	1.11 ± 0.03	0.83 ± 0.02	0.81 ± 0.02	0.66 ± 0.01	0.52 ± 0.01
HBI	1.43 ± 0.01	1.69 ± 0.01	1.55 ± 0.01	0.72 ± 0.00	0.56 ± 0.01
CrI [%]	87.8	87.7	80.6	65.9	56.3

2.4.2. X-ray diffractometry (XRD)

XRD diffractograms of $NBC_1$30, $NBC_3$30 and $NBC_1$65, $NBC_3$65 as well as fdBC were recorded in a Philips type X'Pert Pro diffractometer (Eindhoven, The Netherlands) by using Cu Kα radiation at 30 mA and 40 kV. The spectra over the range of 0–45.0° 2θ were recorded at scan rate of 0.02° 2θ/s. The crystallinity index (CrI) of samples was calculated based on the equation proposed by Segal, Creely, Martin, and Conrad (1959):

$$CrI = \frac{I_{200} - I_{am}}{I_{200}} \times 100$$

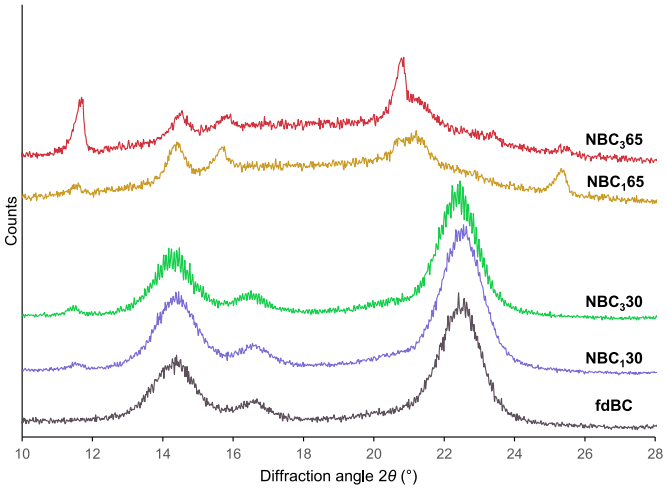

Fig. 2. XRD patterns of fdBC and BC nanocrystals.

where I_{200} and I_{am} are the maximum intensities of diffraction at 2θ = 22,7 and 18°, respectively.

2.4.3. Thermogravimetric analysis

The effect of acid hydrolysis of fdBC on its thermal properties was studied by thermogravimetric analysis using TA Instrument SDT Q600 (New Castle, DE). Samples of 10–20 mg were heated in open aluminum pans under a nitrogen atmosphere within a temperature range of 40–700 °C, at a heating rate of 10 °C/min. Before analysis all samples were conditioned for 7 days in a desiccator over P_2O_5 to remove residual moisture.

2.4.4. Scanning electron microscopy (SEM)

The surface morphology of the fdBC as well as $NBC_1$30, $NBC_3$30 and $NBC_1$65, $NBC_3$65 was observed by SEM (FEI Quanta FEG 250, Thermo Fisher Scientific, Waltham, MA, USA) equipped with a secondary electron detector, operating in high vacuum mode at an accelerating voltage of 10–20 kV.

2.4.5. Conductometric titration

The conductometric titration was carried out to determine the surface charge density (Kalashnikova, Bizot, Cathala, & Capron, 2012; Li et al., 2018). 20 mL 0.1% w/v of degassed suspension of fdBC, $NBC_1$30, $NBC_3$30, $NBC_1$65, and $NBC_3$65 was titrated with 1.0 mM NaOH at a feed rate of 0.1 mL/min. The changes in conductivity were recorded using a conductivity meter (Tetra Con® 325, WTW, Germany).

2.4.6. Contact angle measurement

To determine the contact angle (θ) of fdBC and all BC nanocrystals obtained, their suspensions (approximately 0.5% w/v) were layered onto glass slides and dried at 37 °C to ensure flat and smooth films. The contact angles were measured using the falling drop technique with an Attension Theta Lite goniometer (Nanoscience Instruments, Phoenix, AZ, USA). A 2 μL drop volume of the ultrapure water was deposited on the film surfaces from a micro-syringe (Hamilton-Bonaduz) and left in contact for 10 s at 25 ± 1 °C while being recorded by the equipment's video camera. The presented results represent the average of 5 independent repetitions.

2.5. Emulsion preparation

Aqueous 0.3 and 0.9% suspensions of wBC, fdBC, and XG chosen as a reference stabilizer were prepared and allowed to swell for 24 h. Then, suspensions were mixed with refined olive oil (O) in proportions to yield O/W emulsions having 10, 20, or 30% (v/v) olive oil (Table 1) and

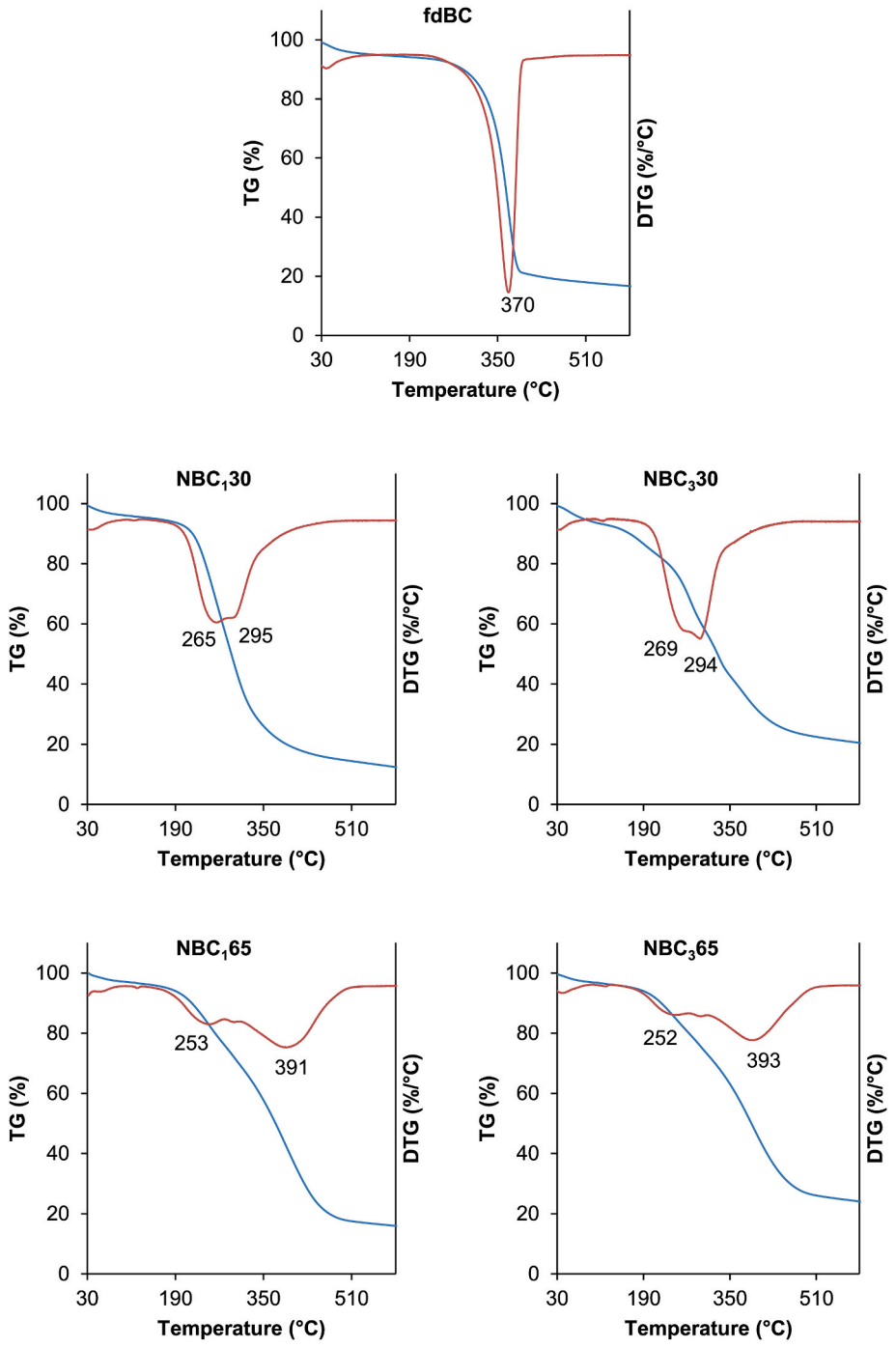

Fig. 3. Thermograms of fdBC and BC nanocrystals: TG curve —, DTG curve.—

sonicated for 1 min at 500 W power and 80% amplitude (VCX 130, Vibra Cell, USA). In a similar way, emulsions stabilized with nanocrystals, i.e., $NBC_1$30, $NBC_3$30 and $NBC_1$65, $NBC_3$65, were prepared, using selected concentrations of stabilizers and olive oil: aqueous 0.3% suspensions of BC nanocrystals were mixed with O in proportions to yield O/W emulsions having 20% olive oil.

The emulsifying properties of all emulsions with the stabilizer addition were compared with those determined for O/W emulsions without any stabilizer.

2.6. Emulsion characteristics

The emulsion stability index (ESI) was assessed according to BN-696060-03 (1969) using the following equation:

$$ESI = He / Hc \bullet 100\%$$

where He is the height of the emulsified layer and Hc is total sample height.

The ESI of emulsions with the addition of wBC, fdBC, and XG was measured immediately. However, as the emulsions undergo unfavorable phenomena over storage time (e.g., coalescence, flocculation, Ostwald ripening), their ESI 24 h after sonication and after centrifugation (10,000 rpm, 5 min) performed in order not to further extend the storage time but to accelerate emulsion breakdown was also determined.

The ESI of emulsions with the addition of BC nanocrystals, i.e., $NBC_1$30, $NBC_3$30 and $NBC_1$65, $NBC_3$65, was determined just after

Table 4
Thermal properties of fdBC and nanocrystals formed after its hydrolysis.

Sample	Temperature range (°C)	Weight loss (%)	DTG peak temperature (°C)
fdBC	35–150	4.1	
	150–510	76.7	370
	510–790	9.0	
	Total	89.8	
$NBC_1$30	35–150	3.9	
	150–510	80.7	267sh, 295
	510–790	6.2	
	Total	90.8	
$NBC_3$30	35–150	3.6	
	150–510	72.9	268sh, 294
	510–790	5.9	
	Total	82.4	
$NBC_1$65	35–150	3.6	
	150–510	78.5	253sh, 391
	510–790	4.3	
	Total	86.4	
$NBC_3$65	35–150	3.6	
	150–510	69.7	252sh, 393
	510–790	5.2	
	Total	78.5	

Table 5
Particles size of fdBC and nanocrystals formed after its hydrolysis with 30% H_2SO_4.

Nanobiber dimension[a]	fdBC	$NBC_1$30	$NBC_3$30	$NBC_1$65	$NBC_3$65
L	977 ± 106	1012 ± 116	1125 ± 120	–[b]	–[b]
D	43.3 ± 13.4	51.4 ± 16.6	67.0 ± 16.7	–	–
L/D	22.6	19.7	16.8	–	–

[a] L – length (nm) and D – diameter of nanobibers
[b] Data not avaiable

sonication and 72 h after sonication. Microscopic images of these emulsions were recorded with the optical microscope (DELTA Optical, DO Evolution 10, Poland).

3. Results and discussion

3.1. Characteristics of the BC nanocrystals obtained

3.1.1. Chemical structure

In the FT-IR spectrum of fdBC, all the bands characteristic of BC were observed. The FT-IR spectra of BC nanocrystals ($NBC_1$30, $NBC_3$30 and $NBC_1$65, $NBC_3$65) were different from the spectrum of fdBC as presented in Fig. 1 and listed in Table 2.

Although spectra of $NBC_1$30 and $NBC_3$30 were similar to that of fdBC, subtle differences in the intensity and shape of the band at the 3650-3000 cm^{-1} region were observed. These differences suggest a change in the H-bonding pattern in $NBC_1$30 and $NBC_3$30 that occurred because of the fdBC hydrolysis.

In the spectra of $NBC_1$65 and $NBC_3$65 more pronounced differences were observed. A significant decrease in the intensity of bands at the 3650-3000 cm^{-1} and 1100-1000 cm^{-1} regions was evident. As the bands in these regions correspond to O–H stretching (ν_{OH}) and C–OH bending (δ_{C-OH}) vibrations, respectively (Table 2), Gromov et al. (2018), Liang, Chen, Wu, Liu, and Lei (2018) and Zhang, Geng, and Yu (2011) suggest that the decrease in their intensity can be indicative of cellulose dehydration. Kuznetsov et al. (2015) and Wang, Li, Zheng, Normakhamatov, and Guo (2007) imply that the decrease in the intensity at the 1100-1000 cm^{-1} region shows the substitution of hydroxyl groups with sulfate groups. The formation of the latter was clearly pointed out by the new positive bands appearing in the differential spectra of $NBC_1$65 and $NBC_3$65 at the 1250-1150 cm^{-1} and 850-750 cm^{-1} regions (Fig. 1). The positive bands in this first region, although of lower intensity, were also observed in differential spectra of $NBC_1$30 and $NBC_3$30. The observed change was also a shift of the band located at 1427 cm^{-1} in the fdBC, $NBC_1$30 and $NBC_3$30 spectra by about 30 cm^{-1} towards higher wave numbers in the $NBC_1$65 and $NBC_3$65 spectra. According to Oh, Yoo, Shin, Kim, et al. (2005) and Colom, Carrillo, Nogués, and Garriga (2003), that absorbance band is very sensitive to the amount of the crystalline vs. amorphous structure of cellulose, and its shift towards higher wave numbers reflects a higher amount of disordered structure in cellulose. The authors concluded that this occurs when cellulose I is converted to cellulose II by mercerization (alkali treatment of cellulose).

Based on the calculated HBI, LOI, and TCI indexes, qualitative changes in the cellulose crystallinity were estimated (Table 3). The HBI index in fdBC increased by the hydrolysis with 30% H_2SO_4 ($NBC_1$30 and $NBC_3$30) and decreased by the hydrolysis with 65% H_2SO_4 ($NBC_1$65 and $NBC_3$65), with the longer reaction time reducing these changes when the lower acid concentration was used and enhancing them when the higher acid concentration was used. As the HBI index is related to the crystal system and the degree of intermolecular regularity as well as the amount of bound water (Kljun et al., 2011), it can be assumed that the crystallinity of $NBC_1$30 and $NBC_3$30 was close to or slightly higher than that of fdBC, while the crystallinity of $NBC_1$65 and $NBC_3$65 was lower than fdBC. At the same time, the LOI and TCI indexes decreased, more pronounced when a higher concentration of H_2SO_4 was used. Unlike the increased HBI index for $BNC_1$30 and $BNC_3$30, the reduced LOI and TCI indexes of all BC nanocrystals could suggest that they had a lower degree of crystallinity (Hurtubise & Krassig, 1960; Kljun et al., 2011; Kruer-Zerhusen, Cantero-Tubilla, & Wilson, 2018; Nada et al., 2000). Such changes in the structure of cellulose were revealed when native cellulose fibers were treated with a strongly alkaline rather than an acidic solution which was associated with a change in the cellulose I to cellulose II ratio. However, according to Xing et al. (2018), at certain concentrations of inorganic acids, cellulose swells and its allomorphic transformation occurs, resembling the mercerization effect induced by strong alkalis. The authors believe that this effect depends on the reaction time of the acid hydrolysis and involves cellulose swelling due to the formation of cellulose sulfate and regeneration to a more thermodynamically stable crystalline form of cellulose II. The formation of cellulose sulfate was confirmed by the FT-IR results for $NCB_1$65 and $NCB_3$65. In turn, according to Nelson and O'Connor (1964b), the spectrum of cellulose II resembles that of cellulose III, although the band at 1163 cm^{-1} appears at the same location in the spectra of cellulose I and cellulose III but is shifted towards lower wave numbers in the spectrum of cellulose II. In the all spectra of Fig. 1 this band appears at the same location, at 1163 cm^{-1}. Moreover, according to French and Santiago Cintrón (2013), when cellulose is treated with H_2SO_4, the higher cellulose depolymerization, due to higher acid concentration used, decreases the TCI index of nanocrystals obtained due to the decrease in the crystal size.

Thus, to get more information on the crystallinity change that occurs in the fdBC under H_2SO_4 used, fdBC and BC nanocrystals were subjected to XRD and thermal analysis.

3.1.2. Crystal structure

The analysis of diffraction pattern of the fdBC and BC nanocrystals confirmed changes in the cellulose structure caused by hydrolysis with H_2SO_4.

In the diffraction pattern of the fdBC two sharp intense diffraction peaks at 2θ around 14.4 and 22.4° and one minor diffraction peak at 2θ around 16.5° (Fig. 2), corresponding to $1\bar{1}0$, 200, and 110 lattice planes, respectively, were assigned as the characteristic diffraction peaks of cellulose I (Sommer, Dederko-Kantowicz, Staroszczyk, Sommer, & Michalec, 2021; Xing et al., 2018). The diffraction patterns of $NBC_1$30 and $NBC_3$30 resembled the fdBC pattern, but in addition to the clearly

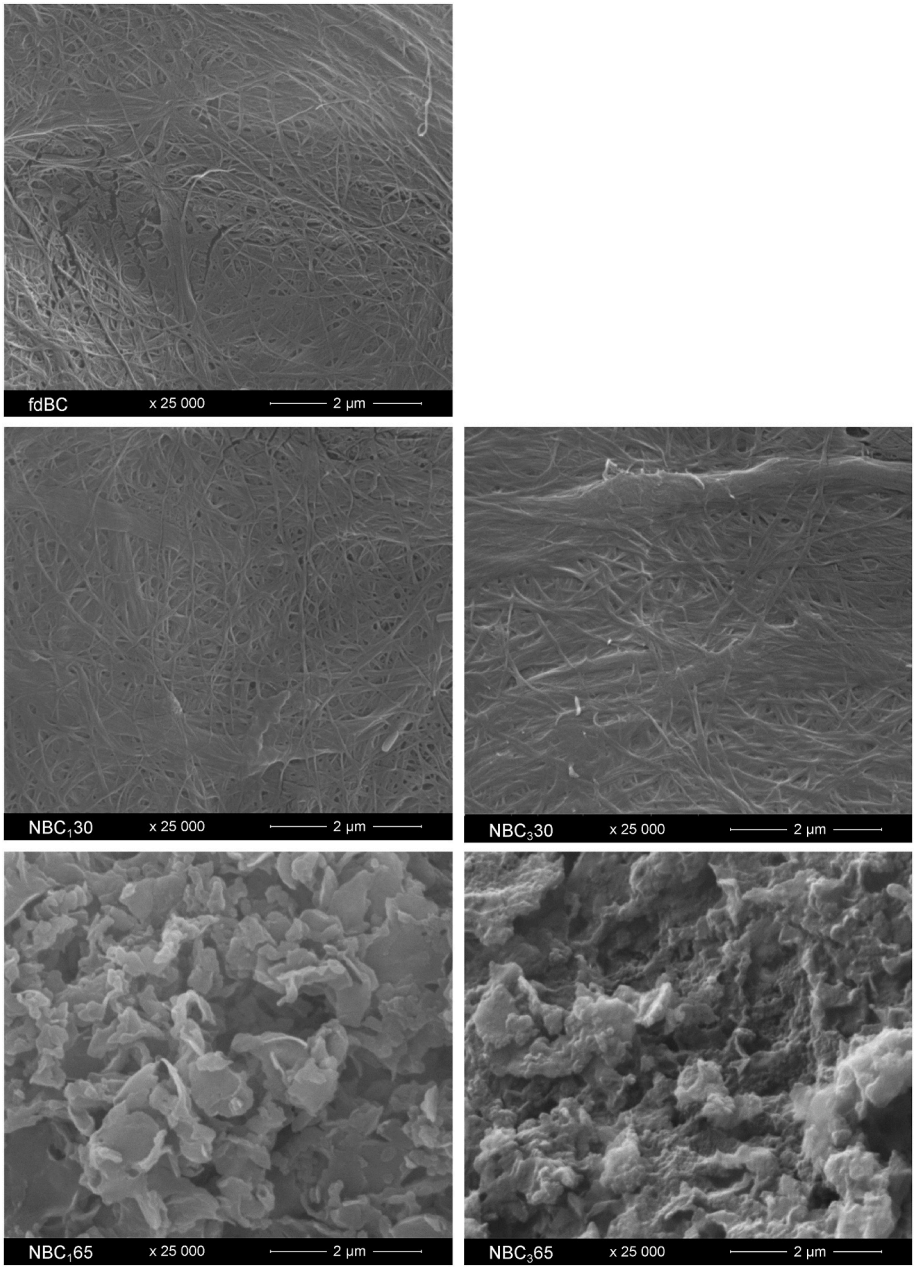

Fig. 4. SEM images of fdBC and BC nanocrystals.

observed three peaks attributed to the crystalline structure of cellulose I, a new low-intensity peak at 2θ around 11.4° appeared in both patterns. In the NBC$_1$65 and NBC$_3$65 diffraction patterns this peak was also observed, especially in the latter, where it became more intense. According to Gong et al. (2017), this peak corresponds to lattice plane 010 of cellulose III. Also, the peak at 2θ around 21° with the shoulder at 21.2° that was observed in the NBC$_1$65 and NBC$_3$65 patterns, according to French (2014) corresponds to a composite of (100), (012), (1$\bar{1}$0) planes of cellulose III$_I$. In contrast, residual peaks at 2θ around 14.4 16.0, and 22.4° clearly indicated the presence of cellulose I in these nanocrystals. The observed changes allow to conclude that the hydrolysis of fdBC with H_2SO_4 leads to a change of the crystal form from cellulose I to cellulose III$_I$ rather than cellulose II and this change is higher when 65% than 30% H_2SO_4 is used.

The CrI of fdBC was high and amounted to 87.8% (Table 3). Thus, the fairly small change in the CrI for NBC$_1$30 and NCB$_3$30 can be attributed to the high crystallinity of the fdBC itself. On the other hand, the low CrI of NBC$_1$65 and NBC$_3$65 indicated that the polymorphic transformation of cellulose I to cellulose III$_I$ could lead to a decrease in crystallinity. According to Vasconcelos et al. (2017), hard hydrolysis conditions (long reaction time, high reaction temperature, high acid concentration) lead to a decrease in the degree of crystallinity of BC nanocrystals in relation to BC due to the tendency to degrade also crystalline BC regions, possibly as a result of a change in the orientation of cellulose chains.

3.1.3. *Thermal properties*

A fast, one-step decomposition of the fdBC took place at 370 °C (Fig. 3) with a 77% weight loss within the temperature range of 150–510 °C (Table 4).

The thermal decomposition of BC nanocrystals was more complex. In general, they held less water than fdBC as indicated by the lower weight loss in the temperature range of 35–150 °C (Table 4), and showed an additional thermal effect as demonstrated by the shoulder on a low-temperature side of the DTG peak (Fig. 3). Analysis of the TG patterns

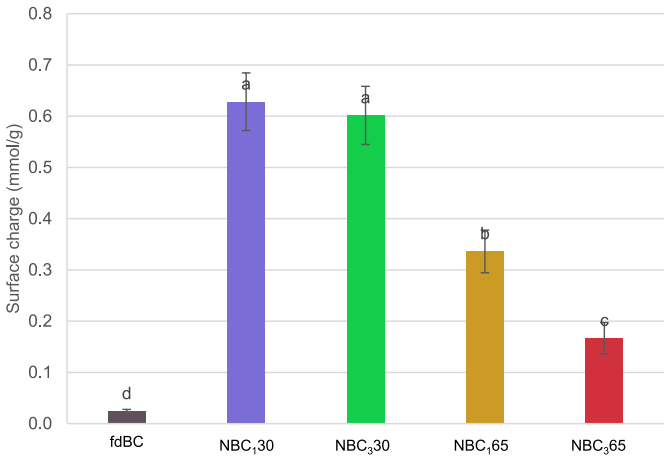

Fig. 5. Charge density of fdBC and BC nanocrystals.

might suggest that this shoulder reflected the thermal degradation of cellulose sulfate regions with maximum of degradation at least 100 °C lower than that of fdBC. In turn, the main DTG peak was related to the more thermally stable fraction of BC nanocrystals, resulting from acid hydrolysis-resistant cellulose, with a degradation maximum at about 75 °C lower or 22 °C higher when using 30 or 65% H_2SO_4, respectively. These results are in accord with former findings. Chemical structures with anhydroglucose sulfate groups on the BC nanocrystal surface are characterized by a higher surface area and lower activation energy of thermal degradation than the parent cellulose (George, Bawa, & Siddaramaiah, 2010, 2011; Roman & Winter 2004; Vasconcelos et al., 2017). George, Ramana, Bawa, and Siddaramaiah (2011) also claim that H_2SO_4 facilitates the decomposition or depolymerization of BC by removing some of the hydroxyl groups either by direct catalysis or by an esterification mechanism.

3.1.4. Surface morphology

The fdBC nanofibers, with an average length (L) and width (D) of 977 and 43 nm, respectively, and an aspect ratio (L/D) of 22.6 (Table 5), formed an ultrafine network (Fig. 4), like that observed in bacterial cellulose (Sommer, Dederko-Kantowicz, et al., 2021). According to Gama, Gatenholm, and Klemm (2017), cellulose nanofibers interact with each other thorough hydrogen bonding and van der Waals forces to form a porous three-dimensional structure that promotes a large surface area.

The dimensions of the fdBC nanofibers under the influence of 30% H_2SO_4 changed slightly (Table 5), while the nanofibers in the $NBC_1$65 and $NBC_3$65 were no longer observed (Fig. 4). The time of hydrolysis with 30% acid did not significantly affect changes in the aspect ratio (L/D), which is one of the crucial parameters when cellulose crystals are employed as Pickering emulsifiers for stabilizing oil-water interfaces (Arserim-Uçar, Korel, Liu, & Yam, 2021). However, according to Arserim-Uçar et al. (2021), the stability of colloidal systems comprising BC nanocrystals depends not only on their size but also on surface properties. As the fdBC, $NBC_1$30 and $NCB_3$30 showed a similar surface morphology (Fig. 4), in the next step a surface charge density as a parameter governing the emulsifying properties was checked.

3.1.5. Surface charge density

The surface charge density of all samples tested ranged from 0.02 to 0.6 mmol/g and depended on the conditions of the fdBC hydrolysis (Fig. 5). While fdBC exhibited the lowest surface charge density, the $NBC_1$30 and $NCB_3$30 showed the highest value, regardless of the reaction time. The surface charge density of the $NBC_1$65 and $NBC_3$65 was higher than that of fdBC but lower than that of $NBC_1$30 and $NBC_3$30, and decreased with longer hydrolysis times. These observed changes confirm the previous findings (Kalashnikova et al., 2012), and were strongly correlated with those observed from FTIR spectra and TGA thermograms. When concentrated H_2SO_4 reacts with cellulose hydroxyl groups, some negatively charged sulfate groups are introduced by esterification, resulting in sulfated nanocrystals.

3.1.6. Hydrophobicity by contact angles measurement

The contact angle of a water drop deposited on a surface depends on the material's hydrophobicity. No contact angle was observed for fdBC, $NBC_1$30, and $NBC_3$30, most likely due to rapid water absorption and/or its spreading in the thin layer of their films. This indicates high hydrophilicity of these samples. The $NBC_1$65 and $NBC_3$65 exhibited lower hydrophilicity, as it suggested by their FTIR spectra analysis, and the measured θ for their thin films depended on the time of fdBC hydrolysis and was 51° for $NBC_1$65 and 75° $NBC_3$65 (Fig. 6). So, although Chiaoprakobkij, Suwanmajo, Sanchavanakit, and Phisalaphong (2020) state that the material is considered hydrophilic if the θ value is below 90° and hydrophobic if it exceeds 90°, the increasing θ value of $NBC_1$65 and $NBC_3$65 with hydrolysis time indicated their hydrophobicity rather than hydrophilicity. A similar conclusion was drawn by Salajková, Berglund, and Zhou (2012) studying the hydrophobicity of cellulose nanocrystals modified with quaternary ammonium salts.

3.2. Effect of wBC, fdBC and XG addition on the O/W emulsion stability

The ESI of O/W emulsions without the addition of the stabilizer ranged from 50 to 80% (Fig. 7). Regardless of the olive oil content, the lowest ESI values showed emulsions subjected to centrifugation, while those 24 h after sonication had the highest ESI value.

The addition of XG increased the ESI of emulsions, with those with 0.3% XG having the ESI higher than those with 0.9% XG whether the emulsion contained 10, 20, or 30% olive oil. The addition of 0.3% of XG caused the emulsions having 10% olive oil to achieve complete emulsification, which was maintained both 24 h after sonication and after centrifugation (the ESI of these emulsions was 100%). For emulsions with the addition of wBC and fdBC, the opposite trend was observed: those with the addition of 0.9% had higher ESI values than those with 0.3% regardless of the olive oil content. The addition of 0.9% fdBC to

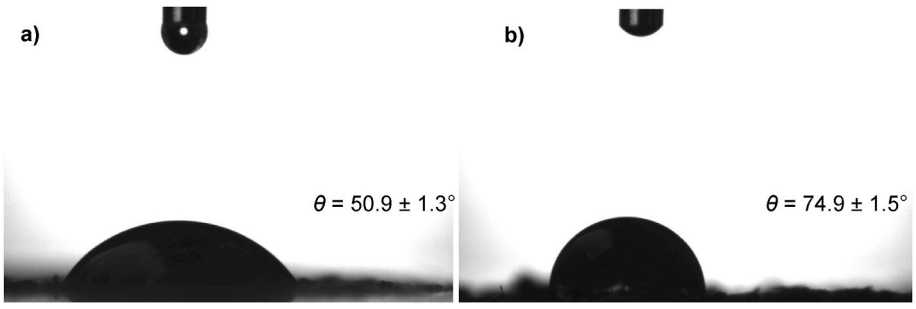

Fig. 6. Micrographs of a water drop on the top of a) $NBC_1$65 and b) $NBC_3$65 thin films.

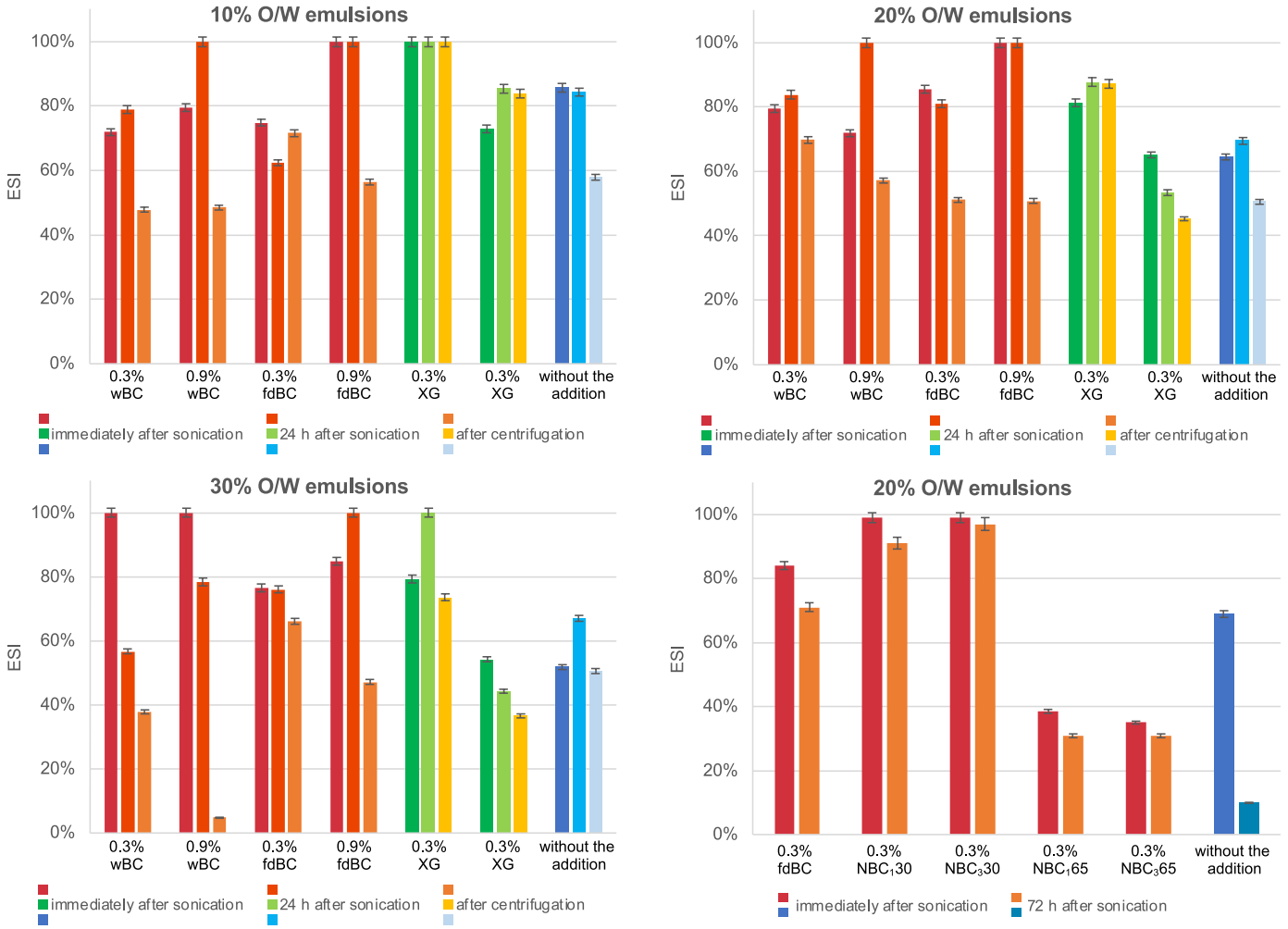

Fig. 7. ESI value of O/W emulsions stabilized with wBC, fdBC, XG, and BC nanocrystals.

emulsions having 10 and 20% olive oil resulted in complete emulsification, which was maintained 24 h after sonication. Like the ESI of the emulsions without any additives, the ESI of emulsions with the wBC and fdBC was the lowest after centrifugation and the highest 24 h after sonication, regardless of the olive oil content.

Paximada, Tsouko, Kopsahelis, Koutinas, and Mandala (2016) showed that O/W emulsions having 10% olive oil and 0.3% of BC addition have an ESI of 92%. The authors measured the ESI after 7 days of storing the emulsions at 4 °C. In contrast, according to Yan et al. (2017), O/W emulsions having 10% olive oil and 0.3 or 0.9% of BC addition have ESI value of 17 or 38%, respectively. In this case, the authors subjected the emulsions to centrifugation. Thus, the concentration of the wBC or fdBC applied affected the emulsion stability and that trend followed the former findings; the higher concentration of the additive used, the higher stability of the resulting emulsion.

Although the emulsions tested were better stabilized with the higher amount of wBC and fdBC (0.9%), the ESI of emulsions having 20% olive oil and containing only 0.3% of wBC or fdBC was higher than the ESI of such emulsion without any additive and with the addition of 0.9% of XG. Therefore, the ability of the BC nanocrystals to stabilize emulsions was tested by preparing emulsions having 20% olive oil and the addition of 0.3% of $NBC_1$30, $NBC_3$30 and $NBC_1$65, $NBC_3$65, and comparing their ESI to the that of the emulsion with the addition of 0.3% fdBC.

3.3. *Effect of BC nanocrystals addition on the O/W emulsion stability*

Observations made on the prepared emulsions indicated that the emulsion without the stabilizer delaminated almost immediately, while those with the addition of fdBC, $NBC_1$30, $NBC_3$30 and $NBC_1$65, $NBC_3$65 did not separate the oil layer even after 72 h of storage. However, the separation of the aqueous layer was evident. Emulsions with the addition of $NBC_1$65 and $NBC_3$65 showed this effect immediately after sonication, and emulsions with the addition of fdBC, $NBC_1$30 and $NBC_3$30 due to storage.

Based on the ESI values it was found that emulsions prepared with the addition of $NBC_1$30 and $NBC_3$30 were the most stable. Their ESI was almost 10 times higher than that of the emulsion without any additive measured 72 h after sonication and 1.2 times higher than the stability of the emulsion with the addition of fdBC. In contrast, the emulsions with the addition of $NBC_1$65 and $NBC_3$65 were 1.3 times less stable than that with the addition of fdBC, but their stability compared to the emulsion without the stabilizer increased 3 times. As it was shown, the BC nanocrystals exhibited strong surface charge density due to sulfated ester moieties. The repulsion forces generated by this negatively charged moieties enabled the formation of stable suspensions (Kalashnikova et al., 2012). The higher surface charge density of particles (Fig. 5), the higher stability of the emulsion.

The microscopic image of emulsions with the addition of fdBC obtained immediately after sonication showed numerous small droplets and occasionally larger ones. No large droplets were observed after 24 h, while small-sized ones were faintly visible. Emulsions with the addition of $NBC_1$30 and $NBC_3$30, both those immediately after sonication and those 24 h afterward, contained droplets of different sizes, but mostly larger than the droplet size of the emulsions with the addition of fdBC.

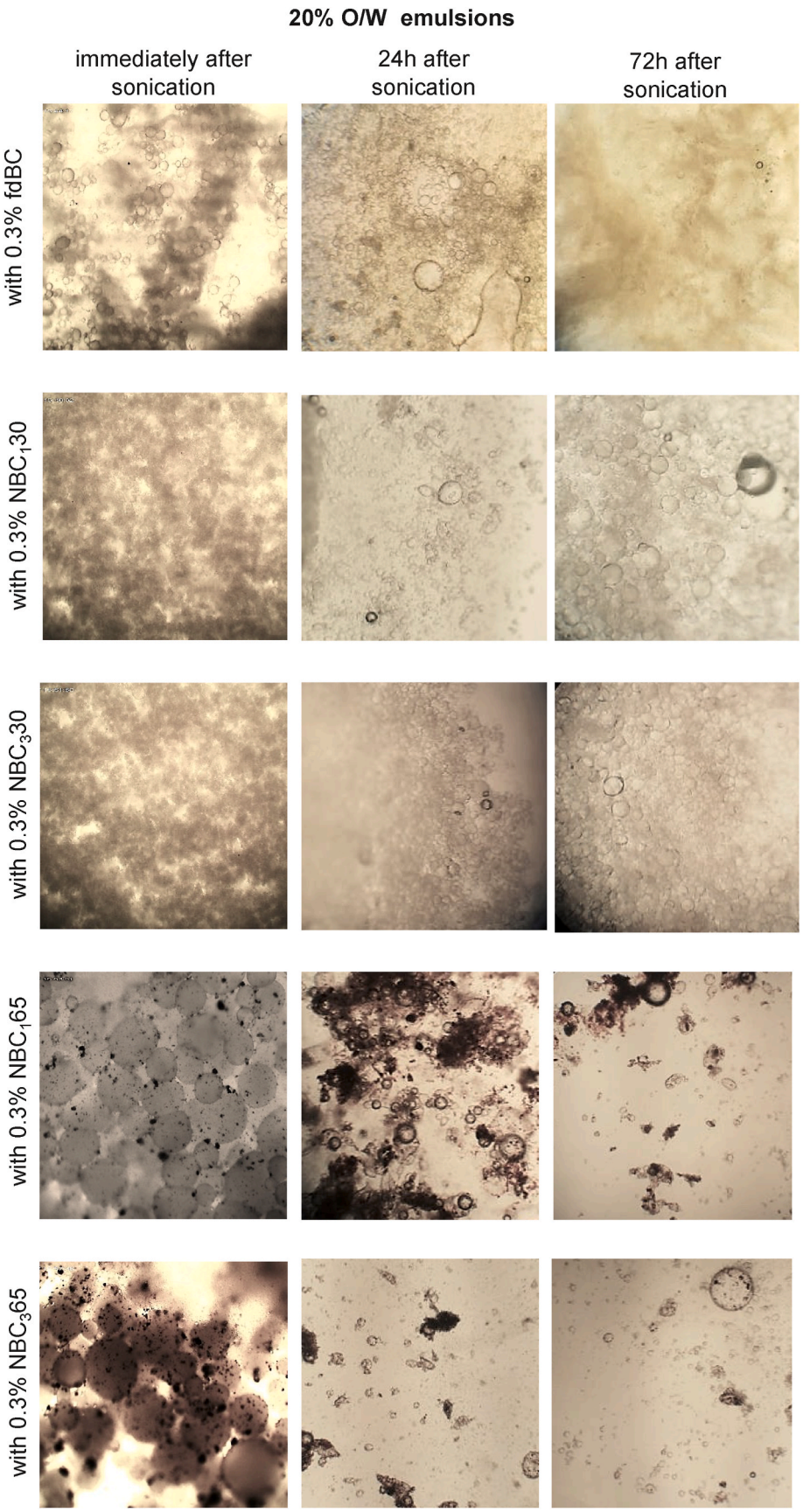

Fig. 8. Optical microscope photos of emulsions having 20% olive oil and the addition of 0.3% fdBC or BC nanocrystal.

Over time, about 2 and 3 times increase in droplet size was observed, which could be due to the Ostwald disproportionation phenomenon (Fig. 8). When comparing the emulsion with the addition of fdBC and those with the addition of $NBC_1$65, $NBC_3$65, up to the 4 times increase in droplet dimensions could be observed. The emulsion with the addition of $NBC_3$65 contained fine droplets of low density with occasional larger droplets that doubled in size after 24 h (Fig. 8).

The droplet size has a key effect on the emulsion rheology. Emulsions with smaller droplets have favorable storage moduli and significantly higher viscosities than emulsions with large droplets (Pal, 1996). Therefore, emulsions with the addition of $NBC_1$65 and $NBC_3$65, with relatively large droplets, are likely to have worse rheological properties than the emulsion with fdBC, while emulsions with the addition of $NBC_1$30 and $NBC_3$30 could potentially exhibit better properties during storage.

4. Conclusions

As the result of the reaction of fdBC with H_2SO_4, nanocrystals with the acid concentration-dependent structure are obtained. The higher concentration of the acid used; the lower crystallinity of the BC nanocrystals obtained with the higher thermal stability at the same time, which is due to the change in the orientation of the cellulose chains. The change in the crystal form from cellulose I to cellulose III_I under the acid used, is higher when 65% than 30% H_2SO_4 is applied. The high crystallinity of native BC ensures the high stability of emulsion with its addition, but lower than that with the addition of XG. Unlike the addition of BC nanocrystals obtained with 65% acid, the addition of those obtained with 30% acid provides the high stability of the O/W emulsion containing up to 20% olive oil. The high emulsion stability was ensured by the strong surface charge density of the nanocrystals obtained with 30% acid resulting from the presence of negatively charged sulfate groups. O/W Pickering emulsion with the addition of BC, either native or in form of nanocrystals obtained with 30% H_2SO_4 can be consider as a novel functional food.

Author contributions

Conceptualization: A.S. and H.S; Experimental runs and analysis: A. S.; Writing: A.S. and H.S. All authors have read and agreed to the published version of the manuscript.

Funding

This work was supported by the Polish national research budget, under the Excellence Initiative - Research University grant number DEC-13/2021/IDUB/I.3.3.

Institutional review board statement

Not applicable.

Declaration of competing interest

The authors declare no conflict of interest.

Data availability

Data will be made available on request.

References

Agarwal, S., Phuoc, T. X., Soong, Y., Martello, D., & Gupta, R. K. (2013). Nanoparticle-stabilised invert emulsion drilling fluids for deep-hole drilling of oil and gas. *Canadian Journal of Chemical Engineering, 91*(10), 1641–1649. https://doi.org/10.1002/cjce.21768

Arserim-Uçar, D. K., Korel, F., Liu, L., & Yam, K. L. (2021). Characterization of bacterial cellulose nanocrystals: Effect of acid treatments and neutralization. *Food Chemistry, 336*, Article 127597. https://doi.org/10.1016/j.foodchem.2020.127597

Beltramino, F., Roncero, M. B., Torres, A. L., Vidal, T., & Valls, C. (2016). Optimization of sulfuric acid hydrolysis conditions for preparation of nanocrystalline cellulose from enzymatically pretreated fibers. *Cellulose, 23*(3), 1777–1789. https://doi.org/10.1007/s10570-016-0897-y

Beltramino, F., Roncero, M. B., Vidal, T., Torres, A. L., & Valls, C. (2015). Increasing yield of nanocrystalline cellulose preparation process by a cellulase pretreatment. *Bioresource Technology, 192*, 574–581. https://doi.org/10.1016/j.biortech.2015.06.007

Binks, B. P. (2007). Emulsions – recent advances in understanding. In B. P. Binks (Ed.), *Modern aspects of emulsion science* (pp. 1–55). The Royal Society of Chemistry.

Björkegren, S., Nordstierna, L., Törncrona, A., & Palmqvist, A. (2017). Hydrophilic and hydrophobic modifications of colloidal silica particles for Pickering emulsions. *Journal of Colloid and Interface Science, 487*, 250–257. https://doi.org/10.1016/j.jcis.2016.10.031

Calabrese, V., Courtenay, J. C., Edler, K. J., & Scott, J. L. (2018). Pickering emulsions stabilized by naturally derived or biodegradable particles. *Curr.Opin. Green Sustain. Chem., 12*, 83–90. https://doi.org/10.1016/j.cogsc.2018.07.002

Capron, I., & Cathala, B. (2013). Surfactant-free high internal phase emulsions stabilized by cellulose nanocrystals. *Biomacromolecules, 14*(2), 291–296. https://doi.org/10.1021/bm301871k

Cheng, H.-L., Liu, H., Feng, Q.-H., Xie, Y.-M., & Zhan, H.-Y. (2017). Preparation, characterization and in vitro anticoagulant activity of corn stover xylan sulfates. *Journal of Biomaterials Science, Polymer Edition, 28*(3), 271–283. https://doi.org/10.1080/09205063.2016.1264060

Cheon, J., Haji, F., Baek, J., Wang, Q., & Tam, K. C. (2023). Pickering emulsions for functional food systems. *J.Agric. Food Res., 11*, Article 100510. https://doi.org/10.1016/j.jafr.2023.100510

Cherhal, F., Cousin, F., & Capron, I. (2016). Structural description of the interface of Pickering emulsions stabilized by cellulose nanocrystals. *Biomacromolecules, 17*(2), 496–502. https://doi.org/10.1021/acs.biomac.5b01413

Chiaoprakobkij, N., Suwanmajo, T., Sanchavanakit, N., & Phisalaphong, M. (2020). Curcumin-loaded bacterial cellulose/alginate/gelatin as a multifunctional biopolymer composite film. *Molecules, 25*(17), 3800. https://doi.org/10.3390/molecules25173800

Colom, X., Carrillo, F., Nogués, F., & Garriga, P. (2003). Structural analysis of photodegraded wood by means of FTIR spectroscopy. *Polymer Degradation and Stability, 80*(3), 543–549. https://doi.org/10.1016/S0141-3910(03)00051-X

French, A. D. (2014). Idealized powder diffraction patterns for cellulose polymorphs. *Cellulose, 21*(2), 885–896. https://doi.org/10.1007/s10570-013-0030-4

French, A. D., & Santiago Cintrón, M. (2013). Cellulose polymorphy, crystallite size, and the segal crystallinity index. *Cellulose, 20*(1), 583–588. https://doi.org/10.1007/s10570-012-9833-y

Gama, M., Gatenholm, P., & Klemm, D. (2017). *Bacterial nanocellulose: A sophisticated multifunctional material*. Boca Raton, London, New York: CRC Press.

Gardiner, E. S., & Sarko, A. (1985). Packing analysis of carbohydrates and polysaccharides. 16. The crystal structures of celluloses IV I and IV II. *Canadian Journal of Chemistry, 63*(1), 173–180. https://doi.org/10.1139/v85-027

George, J., Bawa, A. S., & Siddaramaiah. (2010). Synthesis and characterization of bacterial cellulose nanocrystals and their PVA nanocomposites. *Advanced Materials Research, 123–125*, 383–386. https://doi.org/10.4028/www.scientific.net/AMR.123-125.383.

George, J., Ramana, K. V., Bawa, A. S., & Siddaramaiah. (2011). Bacterial cellulose nanocrystals exhibiting high thermal stability and their polymer nanocomposites. *International Journal of Biological Macromolecules, 48*, 50–57. https://doi.org/10.1016/j.ijbiomac.2010.09.013

Goh, W. N., Rosma, A., Kaur, B., Fazilah, A., Karim, A. A., & Bhat, R. (2012). Microstructure and physical properties of microbial cellulose produced during fermentation of black tea broth (Kombucha). II. *International Food Research Journal, 19*, 153–158.

Gong, J., Li, J., Xu, J., Xiang, Z., & Mo, L. (2017). Research on cellulose nanocrystals produced from cellulose sources with various polymorphs. *RSC Advances, 7*, 33486–33493. https://doi.org/10.1039/C7RA06222B

Grechishcheva, N. Y., Perminova, I. V., Kholodov, V. A., & Meshcheryakov, S. V. (2017). Stabilization of oil-in-water emulsions by highly dispersed particles: Role in self-cleaning processes and prospects for practical application. *Russian Journal of General Chemistry, 87*, 2166–2180. https://doi.org/10.1134/S1070363217090432

Gromov, N. V., Medvedeva, T. B., Taran, O. P., Bukhtiyarov, A. V., Aymonier, C., Prosvirin, I. P., et al. (2018). Hydrothermal solubilization–hydrolysis–dehydration of cellulose to glucose and 5-hydroxymethylfurfural over solid acid carbon catalysts. *Topics in Catalysis, 61*, 1912–1927. https://doi.org/10.1007/s11244-018-1049-4

Hayashi, J., Sufoka, A., Ohkita, J., & Watanabe, S. (1975). The confirmation of existences of cellulose IIII, IIIII, IVI, and IVII by the X-ray method. *Journal of Polymer Science: Polymer Letters Edition, 13*, 23–27. https://doi.org/10.1002/pol.1975.130130104

Hestrin, S., & Schramm, M. (1954). Synthesis of cellulose by Acetobacter xylinum. II. Preparation of freeze-dried cells capable of polymerizing glucose to cellulose. *Biochemical Journal, 58*, 345–352. https://doi.org/10.1042/bj0580345

Hurtubise, F. G., & Krassig, H. (1960). Classification of fine structural characteristics in cellulose by infared spectroscopy. Use of potassium bromide pellet technique. *Analytical Chemistry, 32*, 177–181. https://doi.org/10.1021/ac60158a010

Jia, Y., Zheng, M., Xu, Q., & Zhong, C. (2019). Rheological behaviors of Pickering emulsions stabilized by TEMPO-oxidized bacterial cellulose. *Carbohydrate Polymers, 215*, 263–271. https://doi.org/10.1016/j.carbpol.2019.03.073

Kalashnikova, I., Bizot, H., Cathala, B., & Capron, I. (2012). Modulation of cellulose nanocrystals amphiphilic properties to stabilize oil/water interface. *Biomacromolecules, 13*, 267–275. https://doi.org/10.1021/bm201599j

Kljun, A., Benians, T. A. S., Goubet, F., Meulewaeter, F., Knox, J. P., & Blackburn, R. S. (2011). Comparative analysis of crystallinity changes in cellulose I polymers using ATR-FTIR, X-ray diffraction, and carbohydrate-binding module probes. *Biomacromolecules, 12*, 4121–4126. https://doi.org/10.1021/bm201176m

Kruer-Zerhusen, N., Cantero-Tubilla, B., & Wilson, D. B. (2018). Characterization of cellulose crystallinity after enzymatic treatment using Fourier transform infrared spectroscopy (FTIR). *Cellulose, 25*, 37–48. https://doi.org/10.1007/s10570-017-1542-0

Kuznetsov, B. N., Kuznetsova, S. A., Levdansky, V. A., Levdansky, A. V., Vasil'eva, N. Y., Chesnokov, N. V., et al. (2015). Optimized methods for obtaining cellulose and cellulose sulfates from birch wood. *Wood Science and Technology, 49*, 825–843. https://doi.org/10.1007/s00226-015-0723-y

Liang, J., Chen, J., Wu, S., Liu, C., & Lei, M. (2018). Comprehensive insights into cellulose structure evolution via multi-perspective analysis during a slow pyrolysis process. *Sustainable Energy Fuels, 2*, 1855–1862. https://doi.org/10.1039/C8SE00166A

Li, X., Li, J., Gong, J., Kuang, Y., Mo, L., & Song, T. (2018). Cellulose nanocrystals (CNCs) with different crystalline allomorph for oil in water Pickering emulsions. *Carbohydrate Polymers, 183*, 303–310. https://doi.org/10.1016/j.carbpol.2017.12.085

Low, L. E., Siva, S. P., Ho, Y. K., Chan, E. S., & Tey, B. T. (2020). Recent advances of characterization techniques for the formation, physical properties and stability of Pickering emulsion. *Advances in Colloid and Interface Science, 277*, Article 102117. https://doi.org/10.1016/j.cis.2020.102117

Mason, T. G., Wilking, J. N., Meleson, K., Chang, C. B., & Graves, S. M. (2006). Nanoemulsions: Formation, structure, and physical properties. *Journal of Physics: Condensed Matter, 18*(41), R635–R666. https://doi.org/10.1088/0953-8984/18/41/R01

de Moraes Crizel, T., Haas Costa, T. M., de Oliveira Rios, A., & Hickmann Flôres, S. (2016). Valorization of food-grade industrial waste in the obtaining active biodegradable films for packaging. *Industrial Crops and Products, 87*, 218–228. https://doi.org/10.1016/j.indcrop.2016.04.039

Nada, A.-A. M. A., Kamel, S., & El-Sakhawy, M. (2000). Thermal behaviour and infrared spectroscopy of cellulose carbamates. *Polymer Degradation and Stability, 70*, 347–355. https://doi.org/10.1016/S0141-3910(00)00119-1

Nelson, M. L., & O'Connor, R. T. (1964a). Relation of certain infrared bands to cellulose crystallinity and crystal lattice type. Part II. A new infrared ratio for estimation of crystallinity in celluloses I and II. *Journal of Applied Polymer Science, 8*, 1325–1341. https://doi.org/10.1002/app.1964.070080323

Nelson, M. L., & O'Connor, R. T. (1964b). Relation of certain infrared bands to cellulose crystallinity and crystal latticed type. Part I. Spectra of lattice types I, II, III and of amorphous cellulose. *Journal of Applied Polymer Science, 8*, 1311–1324. https://doi.org/10.1002/app.1964.070080322

Oh, S. Y., Yoo, D. I., Shin, Y., Kim, H. C., Kim, H. Y., Chung, Y. S., et al. (2005). Crystalline structure analysis of cellulose treated with sodium hydroxide and carbon dioxide by means of X-ray diffraction and FTIR spectroscopy. *Carbohydrate Research, 340*, 2376–2391. https://doi.org/10.1016/j.carres.2005.08.007

Oh, S. Y., Yoo, D. I., Shin, Y., & Seo, G. (2005). FTIR analysis of cellulose treated with sodium hydroxide and carbon dioxide. *Carbohydrate Research, 340*, 417–428. https://doi.org/10.1016/j.carres.2004.11.027

Ozturk, B., & McClements, D. J. (2016). Progress in natural emulsifiers for utilization in food emulsions. *Current Opinion in Food Science, 7*, 1–6. https://doi.org/10.1016/j.cofs.2015.07.008

Pal, R. (1996). Effect of droplet size on the rheology of emulsions. *AIChE Journal, 42*, 3181–3190. https://doi.org/10.1002/aic.690421119

Pang, B., Liu, H., & Zhang, K. (2021). Recent progress on Pickering emulsions stabilized by polysaccharides-based micro/nanoparticles. *Advances in Colloid and Interface Science, 296*, Article 102522. https://doi.org/10.1016/j.cis.2021.102522

Paximada, P., Tsouko, E., Kopsahelis, N., Koutinas, A. A., & Mandala, I. (2016). Bacterial cellulose as stabilizer of o/w emulsions. *Food Hydrocolloids, 53*, 225–232. https://doi.org/10.1016/j.foodhyd.2014.12.003

Pereira, B., & Arantes, V. (2020). Production of cellulose nanocrystals integrated into a biochemical sugar platform process via enzymatic hydrolysis at high solid loading. *Industrial Crops and Products, 152*, Article 112377. https://doi.org/10.1016/j.indcrop.2020.112377

Peter, Z. (2021). Order in cellulosics: Historical review of crystal structure research on cellulose. *Carbohydrate Polymers, 254*, Article 117417. https://doi.org/10.1016/j.carbpol.2020.117417

Roman, M., & Winter, W. T. (2004). Effect of sulfate groups from sulfuric acid hydrolysis on the thermal degradation behavior of bacterial cellulose. *Biomacromolecules, 5*, 1671–1677. https://doi.org/10.1021/bm034519+

Salajková, M., Berglund, L. A., & Zhou, Q. (2012). Hydrophobic cellulose nanocrystals modified with quaternary ammonium salts. *Journal of Materials Chemistry, 22*, Article 19798. https://doi.org/10.1039/c2jm34355j

Segal, L., Creely, J. J., Martin, A. E., & Conrad, C. M. (1959). An empirical method for estimating the degree of crystallinity of native cellulose using the X-Ray diffractometer. *Textile Research Journal, 29*, 786–794. https://doi.org/10.1177/004051755902901003

Shahabi-Ghahafarrokhi, I., Khodaiyan, F., Mousavi, M., & Yousefi, H. (2015). Preparation and characterization of nanocellulose from beer industrial residues using acid hydrolysis/ultrasound. *Fibers and Polymers, 16*, 529–536. https://doi.org/10.1007/s12221-015-0529-4

Shah, N., Ul-Islam, M., Khattak, W. A., & Park, J. K. (2013). Overview of bacterial cellulose composites: A multipurpose advanced material. *Carbohydrate Polymers, 98*, 1585–1598. https://doi.org/10.1016/j.carbpol.2013.08.018

Sommer, A., Dederko-Kantowicz, P., Staroszczyk, H., Sommer, S., & Michalec, M. (2021). Enzymatic and chemical cross-linking of bacterial cellulose/fish collagen composites—a comparative study. *International Journal of Molecular Sciences, 22*, 3346. https://doi.org/10.3390/ijms22073346

Sommer, A., Staroszczyk, H., Sinkiewicz, I., & Bruździak, P. (2021). Preparation and characterization of films based on disintegrated bacterial cellulose and montmorillonite. *Journal of Polymers and the Environment, 29*, 1526–1541. https://doi.org/10.1007/s10924-020-01968-5

Surma-Ślusarska, B., Presler, S., & Danielewicz, D. (2008). Characteristics of bacterial cellulose obtained from Acetobacter xylinum culture for application in papermaking. *Fibres and Textiles in Eastern Europe, 4*(69), 108–111.

Tang, Y., Yang, S., Zhang, N., & Zhang, J. (2014). Preparation and characterization of nanocrystalline cellulose via low-intensity ultrasonic-assisted sulfuric acid hydrolysis. *Cellulose, 21*, 335–346. https://doi.org/10.1007/s10570-013-0158-2

Tong, X., Shen, W., Chen, X., Jia, M., & Roux, J. (2020). Preparation and mechanism analysis of morphology-controlled cellulose nanocrystals via compound enzymatic hydrolysis of eucalyptus pulp. *Journal of Applied Polymer Science, 137*, Article 48407. https://doi.org/10.1002/app.48407

Ul-Islam, M., Khan, T., & Park, J. K. (2012). Nanoreinforced bacterial cellulose–montmorillonite composites for biomedical applications. *Carbohydrate Polymers, 89*, 1189–1197. https://doi.org/10.1016/j.carbpol.2012.03.093

Vasconcelos, N. F., Feitosa, J. P. A., da Gama, F. M. P., Morais, J. P. S., Andrade, F. K., de Souza Filho, M. de S. M., et al. (2017). Bacterial cellulose nanocrystals produced under different hydrolysis conditions: Properties and morphological features. *Carbohydrate Polymers, 155*, 425–431. https://doi.org/10.1016/j.carbpol.2016.08.090

Wang, Z. M., Li, L., Zheng, B. S., Normakhamatov, N., & Guo, S. Y. (2007). Preparation and anticoagulation activity of sodium cellulose sulfate. *International Journal of Biological Macromolecules, 41*, 376–382. https://doi.org/10.1016/j.ijbiomac.2007.05.007

Wang, J., Tavakoli, J., & Tang, Y. (2019). Bacterial cellulose production, properties and applications with different culture methods – a review. *Carbohydrate Polymers, 219*, 63–76. https://doi.org/10.1016/j.carbpol.2019.05.008

Xing, L., Gu, J., Zhang, W., Tu, D., & Hu, C. (2018). Cellulose I and II nanocrystals produced by sulfuric acid hydrolysis of Tetra pak cellulose I. *Carbohydrate Polymers, 192*, 184–192. https://doi.org/10.1016/j.carbpol.2018.03.042

Yan, H., Chen, X., Song, H., Li, J., Feng, Y., Shi, Z., et al. (2017). Synthesis of bacterial cellulose and bacterial cellulose nanocrystals for their applications in the stabilization of olive oil pickering emulsion. *Food Hydrocolloids, 72*, 127–135. https://doi.org/10.1016/j.foodhyd.2017.05.044

Yang, J., Du, Y., Wen, Y., Li, T., & Hu, L. (2003). Sulfation of Chinese lacquer polysaccharides in different solvents. *Carbohydrate Polymers, 52*, 397–403. https://doi.org/10.1016/S0144-8617(02)00330-2

Zhai, X., Lin, D., Liu, D., & Yang, X. (2018). Emulsions stabilized by nanofibers from bacterial cellulose: New potential food-grade Pickering emulsions. *Food Research International, 103*, 12–20. https://doi.org/10.1016/j.foodres.2017.10.030

Zhang, M., Geng, Z., & Yu, Y. (2011). Density functional theory (DFT) study on the dehydration of cellulose. *Energy & Fuels, 25*, 2664–2670. https://doi.org/10.1021/ef101619e